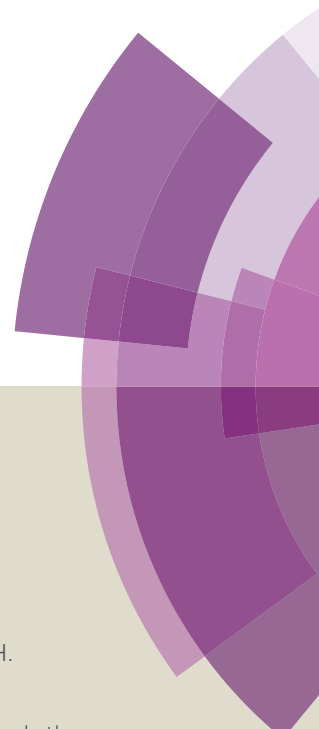


# Journal of Materials Chemistry A

Accepted Manuscript



This article can be cited before page numbers have been issued, to do this please use: Y. Luan, Y. Qi, H. Gao, N. Zheng and G. Wang, *J. Mater. Chem. A*, 2014, DOI: 10.1039/C4TA04311A.



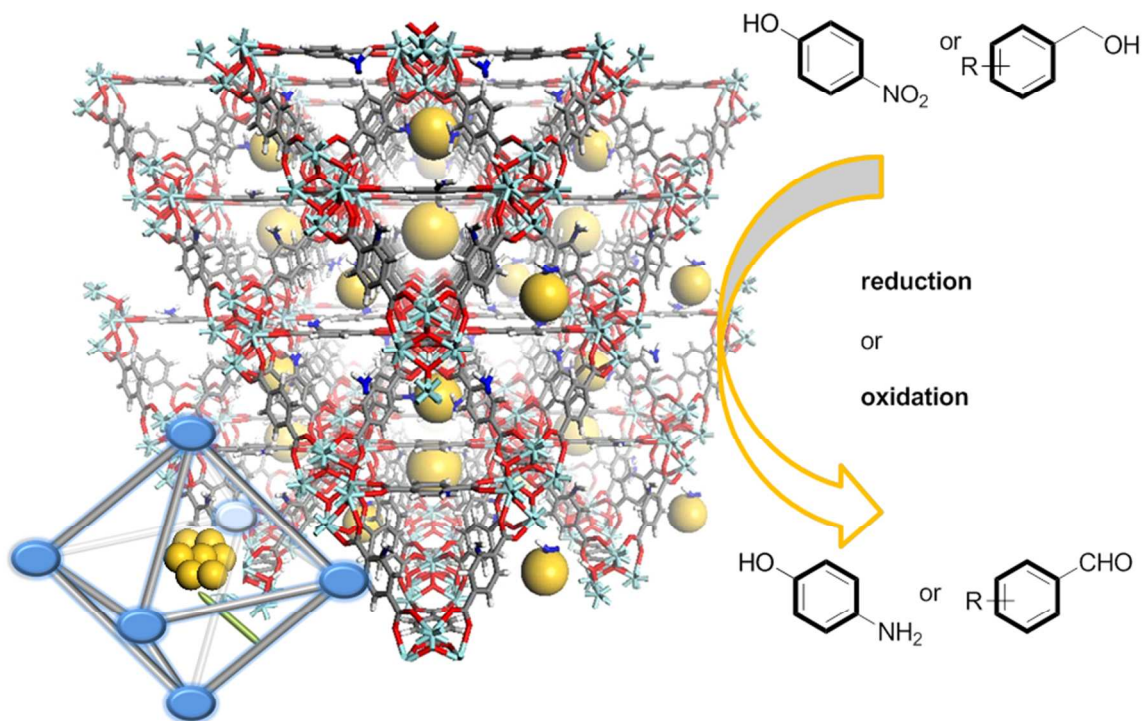
This is an *Accepted Manuscript*, which has been through the Royal Society of Chemistry peer review process and has been accepted for publication.

*Accepted Manuscripts* are published online shortly after acceptance, before technical editing, formatting and proof reading. Using this free service, authors can make their results available to the community, in citable form, before we publish the edited article. We will replace this *Accepted Manuscript* with the edited and formatted *Advance Article* as soon as it is available.

You can find more information about *Accepted Manuscripts* in the [Information for Authors](#).

Please note that technical editing may introduce minor changes to the text and/or graphics, which may alter content. The journal's standard [Terms & Conditions](#) and the [Ethical guidelines](#) still apply. In no event shall the Royal Society of Chemistry be held responsible for any errors or omissions in this *Accepted Manuscript* or any consequences arising from the use of any information it contains.

## Table of content



A Au@MOF catalyst for reduction, aerobic oxidation, and N-alkylation reaction sequences has been achieved using a novel absorption/reduction method.

## ARTICLE

# Synthesis of amino-functionalized metal-organic framework at nanoscale for gold nanoparticle deposition and catalysis

Cite this: DOI: 10.1039/x0xx00000x

Yi Luan, Yue Qi, Hongyi Gao, Nannan Zheng and Ge Wang\*

Received 00th January 2012,

Accepted 00th January 2012

DOI: 10.1039/x0xx00000x

[www.rsc.org/](http://www.rsc.org/)

In this study, highly dispersed Au nanoparticles have been immobilized on amino-functionalized metal-organic frameworks (MOFs) via a novel absorption/reduction method in solution. The amino functionality of the MOF rapidly coordinated with  $\text{HAuCl}_4$  and acted as the Au(0) precursor in the absence of protecting agents. The resulting Au@MOF catalyst was well dispersed in aqueous media taking advantage of its well-defined and uniform sizes and nanomorphologies. The as-synthesized Au@MOF catalyst exhibited high catalytic activities in a wide variety of reactions under ambient conditions, such as the base-free aerobic oxidation of alcohols and a oxidation/imine formation/reduction reaction sequences. Furthermore, the Au@MOF catalyst can be easily recovered and reused several times without leaching of metals or significant loss of activity.

## Introduction

Metal-organic frameworks (MOFs) are emerging as important functional materials for gas storage, separation, heterogeneous catalysis, sensing and drug delivery due to their high surface area, porosity and chemical tunability.<sup>1,2</sup> Owing to these features, the applications of MOFs in heterogeneous catalysis have recently attracted tremendous attention.<sup>3-5</sup> Likewise, the use of metal nanoparticles to catalyze organic chemistry transformations has attracted great interest in recent years.<sup>6</sup> Various materials, such as polymers<sup>7,8</sup> and inorganic oxides,<sup>9</sup> have been employed as supports in order to prevent the agglomeration of the metal nanoparticles. Recently, MOFs have been utilized as a new type of support for noble metal nanoparticles.<sup>10-12</sup> The combination of the solid porous structure of MOFs and the high catalytic activities of metal nanoparticles offers advantages over other catalysts, such as shorter reaction times and excellent recyclability.<sup>13</sup>

Several methods for loading metal nanoparticles into porous MOFs using an assortment of techniques have been recently reported, such as solid grinding,<sup>14,15</sup> chemical vapor deposition,<sup>16</sup> incipient wetness impregnation<sup>17</sup> and solution infiltration.<sup>18,19</sup> A solution-based synthetic approach to MOFs is preferred because it can be easily carried out in lab or on a large scale.<sup>20</sup> Férey introduced ethylenediamine grafting onto MIL-101(Cr) for the encapsulation of noble metal nanoparticles.<sup>21</sup> Cao reported several Pd@MOF materials using a direct anionic exchange approach for palladium nanoparticle encapsulation.<sup>22,23</sup> Among metal and metal oxide nanoparticles, gold nanoparticles have become one of the most intensely studied catalysts beginning with the discovery of low-

temperature CO oxidation over Au nanoparticles (NPs) supported on base metal oxides.<sup>24,25</sup> In particular, we are interested in the fabrication of gold nanoparticles in nanosized metal-organic frameworks because it may bring new opportunities in the development of highly active heterogeneous gold catalysts.<sup>26</sup>

Although a few examples of MOF-supported gold nanoparticles have been reported, the preparation of active gold nanoparticles deposited on MOF catalysts in solution remains challenging.<sup>27,28</sup> Furthermore, while large amounts of MOF materials have been studied as catalysts, nanoscale MOFs have received much less attention.<sup>29</sup> Nanoscale metal-organic frameworks characteristically show well-defined and uniform sizes and morphologies.<sup>30,31</sup> These features make MOFs at nanoscale excellent catalysts since they can be well dispersed in aqueous media or other solvents.<sup>32,33</sup> Herein, we report a one-pot absorption/reduction synthesis of gold deposited MOFs on the nanoscale, which are functionalized by amino groups for the stabilization of metal nanoparticles. These amino functionalized MOFs can be used for depositing small gold nanoparticles using a solution-based preparation method, which obviates the use of metal stabilizers, such as polyvinylpyrrolidone (PVP).<sup>34</sup> To the best of our knowledge, this work represents the first example of utilizing amine functional groups for the stabilization of Au(0) through a solution-based synthesis approach. In contrast to current literature precedence involving aerobic oxidation reactions and *N*-alkylation reaction sequence promoted by Au(0), our Au@nanosized MOFs catalyst is the first example for a single Au(0) heterogeneous catalyst that promotes multiple catalytic transformations involving oxidation and reduction. The as-synthesized Au@UiO-66(NH<sub>2</sub>) at nanoscale shows excellent

catalytic activities toward base-free aerobic oxidation of alcohols and aerobic oxidation/imine formation/reduction reaction sequences.

## 2. Experimental

### 2.1 Catalyst Preparation

**Preparations of nano IRMOF-3 crystals.** Synthesis of nanoscale IRMOF-3 was achieved using a modified literature procedure.<sup>35</sup> Zn(NO<sub>3</sub>)<sub>2</sub>·4H<sub>2</sub>O (1.44 g, 5.5 mmol), 2-aminoterephthalic acid (0.37 g, 2 mmol), and 50 mL *N,N*-dimethylformamide (DMF) were mixed at room temperature. The obtained solution was sealed and placed in the oven at 55 °C for 96 h. 10 mL of the incubated solution was placed in a reaction flask and cetyltrimethylammonium bromide (CTAB) (0.728 g, 2 mmol) was added with stirring at 55 °C until the CTAB was completely dissolved. The solution was then transferred to another oven at 105 °C and heated for 1.5 h. After the reaction was cooled, triethylamine (TEA) was added (278 μL, 2 mmol) under strong stirring for 10 min. Nanoscale IRMOF-3 products were separated, washed with DMF (3 x 10 mL) and chloroform (3 x 10 mL). The product was immersed in chloroform overnight to remove DMF guest molecules from IRMOF-3 crystals and finally dried under vacuum.

**Preparations of nano UiO-66(NH<sub>2</sub>) crystals.** Synthesis of nanoscale UiO-66(NH<sub>2</sub>) was achieved by using modified literature procedures.<sup>36,37</sup> A mixture of ZrCl<sub>4</sub> (0.4 g, 1.7 mmol) in DMF (75 mL) was reacted with acetic acid (2.85 mL, 850 mmol) at 55 °C. A DMF solution (25 mL) of 2-aminoterephthalic acid (0.311 g, 1.7 mmol) was added to the clear solution. Next, water (0.125 mL, 0.007 mmol) was added to the solution and the solution was sonicated at 60 °C and kept in a bath at 120 °C for 24 h. After 24 h, the solution was cooled to room temperature and the precipitate was collected by centrifugation. The obtained solid was washed with DMF (2 x 10 mL), ethanol (3 x 10 mL) and dried under reduced pressure (80 °C, 3 h). Our synthesized nanoscale UiO-66(NH<sub>2</sub>) exhibited excellent mechanical stability.<sup>38</sup>

**Preparations of nano Cr-MIL-101(NH<sub>2</sub>) crystals.** The synthesis of nanoscale Cr-MIL-101(NH<sub>2</sub>) was not successful using 2-aminoterephthalic acid as the organic ligand with the control of the nanomorphology. It was expected that the synthesis of nanoscale Cr-MIL-101(NH<sub>2</sub>) could be achieved starting from nanoscale MIL-101. However, the post-synthetic modification of Cr-MIL-101 approach was not utilized because it added several extra steps towards the MOF synthesis with the involvement of environmentally hazardous Cr(NO<sub>3</sub>)<sub>3</sub>·9H<sub>2</sub>O and SnCl<sub>2</sub> reagents.<sup>39</sup>

**Preparations of Au@IRMOF-3 crystal by solution-based synthesis method.** Nanoscale IRMOF-3 crystals (0.5 g) were dispersed into a solvent mixture of absolute ethanol (50 mL) and deionized water (50 mL) in a flask. After being transferred into a 250 mL three-necked flask, HAuCl<sub>4</sub> (2.5 mL, 0.025 M aqueous solution) was added and stirred mechanically in an ice bath for 4 h followed by addition of a NaBH<sub>4</sub> aqueous solution (10 mL, 0.05 M aqueous solution). The reaction was incubated at 0 °C for 0.5 h, and the resulting product was separated through centrifugation and washed with water (3 x 15 mL).

**Preparations of Au@UiO-66(NH<sub>2</sub>) crystal by solution-based synthesis method.** The procedure was the same as the aforementioned preparation of Au@IRMOF-3 except nanoscale UiO-66(NH<sub>2</sub>) crystals were used instead of IRMOF-3 crystals.

### 2.2. Characterization.

The phase composition of the samples was investigated by X-ray powder diffraction (XRD, M21X, Cu Kα radiation, λ=0.154178 nm). The morphology and structure of the as-obtained product were characterized by scanning electron microscopy (SEM, ZEISS SUPRA55). Further information about the structure was revealed by transmission electron microscopy (TEM, TEI Tecnai F20) and high-resolution TEM (HRTEM, TEI Tecnai F20) using TEI Tecnai F20. The samples for the SEM, TEM and HRTEM measurements were first dispersed in ethanol and sonicated for a few minutes then supported onto the silicon slice and the holey carbon film on a Cu grid, respectively. The chemical compositions were analyzed using X-ray photoelectron spectrometer (XPS, ESCALAB 250Xi) and inductively coupled plasma-atomic emission spectrometry (ICP-AES, Vavian 715-ES). Thermogravimetric analysis (TG) was conducted by Netzsch STA449F at a heating rate of 10 °C/min under the N<sub>2</sub> flow. The specific surface areas were calculated by nitrogen sorption-desorption isotherms using a Micromeritics ASAP 2420 adsorption analyzer. The pore size distributions were derived from the adsorption branches of isotherms by using the Barrett-Joyner-Halenda (BJH) model. Fourier transform infrared spectroscopy (FTIR) was acquired on Nicolet 6700 using the KBr pellet technique. The results were analyzed by gas chromatography-mass spectrometry using an internal standard (GC-MS, Agilent7890/5975C-GC/MSD, HP5-MS column, Ar carrier gas, 200 °C).

### 2.3. Catalytic performance evaluation.

**Aerobic Oxidation of Alcohols.** The catalytic activity of all of the prepared catalysts in the aerobic oxidation of alcohols was evaluated by running the reactions in a 25 mL flask with a reflux condenser. In a typical reaction, the flask was first charged with desired amount of alcohol, catalyst and NaHCO<sub>3</sub>. After purging three times with oxygen and setting up with an oxygen balloon, the closed vessel was heated rapidly to reach the desired reaction temperature. After 1 h, the flask was cooled to room temperature. The filtered liquid samples were quantitatively analyzed by gas chromatography using nitrobenzene as the standard without aqueous work-up. A calibration curve for each reactant and product has been built, which is included in the supporting information. The in-situ <sup>1</sup>H NMR monitoring of reaction conversion and yield was performed in DMF-d<sub>7</sub> solvent. The crude sample was filtered and transferred to an NMR tube for direct <sup>1</sup>H NMR analysis. Furthermore, all aldehyde products were isolated through column chromatography and the isolated yields were provided.

**Oxidation/Imine Formation/Reduction Sequence.** A 25 mL flask with a reflux condenser was charged with a magnetic stirring bar, benzyl alcohol (1.0 mmol), aniline (1.0 mmol), Au catalyst (1.0 mol%), NaHCO<sub>3</sub> (1.0 mmol), and xylenes (3.0 mL). The mixture

was stirred under a  $N_2$  atmosphere at 130 °C for 12 h, followed by the addition of 2-propanol (6.0 mmol) and then stirred for another 36 h. The reaction mixture was washed with  $H_2O$ , extracted with  $Et_2O$ , dried over  $Na_2SO_4$ , filtered, and analyzed by GC-MS and GC using anisole as an internal standard.

#### 2.4. Catalyst Recycling.

For catalyst recycling experiments, the reactions were performed under the same reaction conditions each time using the recovered catalyst from the previous run. The catalyst was filtered and washed with DMF before reuse. To study the leaching of Au during the reaction, the mother liquor was analyzed by ICP-AES and re-evaluated under catalytic conditions.

### 3. Results and Discussion

#### 3.1. Characterization of Nano-MOFs Material

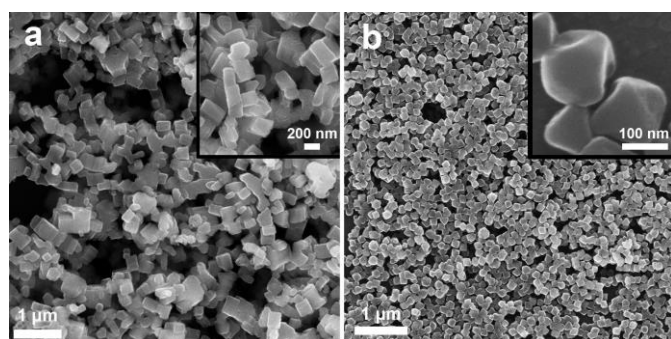
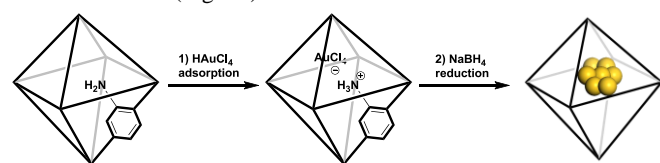


Fig. 1 SEM images of nanoscale IRMOF-3 (a) and UiO-66(NH<sub>2</sub>) (b).

The successful synthesis of nanoscale IRMOF-3 and UiO-66(NH<sub>2</sub>) was achieved according to modified literature procedure. Rectangular cuboid crystals of IRMOF-3 with good monodispersity and crystallinity were successfully produced in very high yield (> 95%). Crystal sizes of about 200-300 nm were observed in the present synthesis at room temperature (Fig. 1a). On the other hand, UiO-66(NH<sub>2</sub>) crystals appear to have an octahedral morphology and a size of 150 nm (Fig. 1b).



Scheme 1 Schematic illustration of the synthesis of the Au@MOF material.

The amino-functionalized MOFs were employed for a good distribution of  $HAuCl_4$  over the outer and inner surfaces of the MOF porous structure. The excellent distribution of  $HAuCl_4$  ensures the gold nanoparticles disperse well over the surface of the nano MOFs. The Au@MOF material was synthesized using  $HAuCl_4$  as the gold precursor in the presence of  $NaBH_4$  (Scheme 1). To demonstrate that  $HAuCl_4$  has been adsorbed onto the MOF support before the  $NaBH_4$  reduction, the reaction solution was monitored by a digital camera, as well as UV-Vis spectroscopy (Fig. S1 and S2). Fig. S2 shows the UV-vis spectra of a  $HAuCl_4$  aqueous solution before and after the effect of the adsorption procedure. A rapid absorption of  $HAuCl_4$

with the disappearance of yellow color, which was not observed in other MOFs without an amino group, suggested the crucial role of the amine group on MOFs for absorption (Fig. S1). The peak of  $[AuCl_4]^-$  ions at 300 nm disappeared rapidly after mixing an amino functionalized MOF support and the  $HAuCl_4$  aqueous solution, which further indicated the absorption of  $[AuCl_4]^-$  ions via an electrostatic interaction between  $NH_3^+$  and  $[AuCl_4]^-$  (Fig. S2).

It was also observed that IRMOF-3 was unstable towards to  $HAuCl_4$  or  $NaBH_4$ , and led to significant decomposition during the loading of gold nanoparticles. This decomposition was confirmed by XRD and HRTEM (Fig. S11 and S12). In this case, UiO-66(NH<sub>2</sub>) was used as a stable support for gold nanoparticles. The great stability of the UiO-66(NH<sub>2</sub>) compared with the IRMOF-3 was an incentive to use the former for heterogeneous catalysis. It is worth mentioning that 2,5-pyridinedicarboxylic acid (pydc) was also employed as the organic ligand for Zr-based Zr(pydc) MOF support. However, no  $HAuCl_4$  absorption with Zr(pydc) MOF was observed, presumably because the pyridine moiety participates in the formation of the main framework of the Zr(pydc) MOF. This result suggested the free amine moiety on UiO-66(NH<sub>2</sub>) was the key for the  $HAuCl_4$  absorption. Treatment of  $UiO-66(NH_3^+)AuCl_4^-$  with  $NaBH_4$  cleanly converted it to the desired Au@UiO-66(NH<sub>2</sub>) material (Scheme 1).

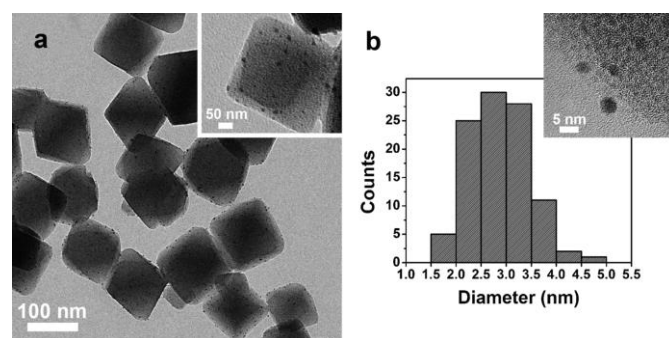


Fig. 2 HRTEM images of 1.8% Au@UiO-66(NH<sub>2</sub>) (a) and size distribution of Au NPs (b), the inset of b is the zoomed TEM image.

The gold distribution for Au@UiO-66(NH<sub>2</sub>) was analyzed by HRTEM. HRTEM images of 1.8 wt% Au@UiO-66(NH<sub>2</sub>) and corresponding size distribution of Au nanoparticles are shown in Fig. 2. The loading of gold nanoparticles did not affect the nano morphology of UiO-66(NH<sub>2</sub>) (Fig. 2a). It was determined that Au NPs were highly dispersed on the Au@UiO-66(NH<sub>2</sub>) with mean diameters of 2.8 nm and 3.1 nm (as estimated by size distribution in Fig. 2b). The proposed formation mechanism of ~3 nm gold nanoparticles is as follows. The formation was initiated by the collection of  $HAuCl_4$  molecules inside the channels, as well as partially on the surface of the host solid. The ion pair  $(NH_3^+)AuCl_4^-$  was stabilized by the amine ligands attached to benzene-1,4-dicarboxylate, and the ion pair was distributed evenly over the MOF channels as the immersion time progressed, until the nanoparticles were formed upon the treatment of  $NaBH_4$ . The EDX and XPS analysis confirm the presence of Au(0) for the Au@UiO-66(NH<sub>2</sub>) sample (Fig. S4 and 4).

The BET surface area and gold loading data of nanoscale MOFs and Au@MOFs are summarized in Table 1. The corresponding

surface area of Au@IRMOF-3 reduced significantly from the parent IRMOF-3 due to the decomposition of IRMOF-3 pores. The gold

**Table 1** The N<sub>2</sub> Adsorption–desorption Isotherms and Au Loading of MOFs<sup>a</sup>

Sample	$S_{\text{BET}}$ (m <sup>2</sup> g <sup>-1</sup> )	$V_{\text{pore}}$ (cm <sup>3</sup> g <sup>-1</sup> )	Au loading
IRMOF-3 <sup>b</sup>	~600	0.44	-
Au@IRMOF-3 <sup>c</sup>	111.4	0.41	1.6 wt%
UiO-66(NH <sub>2</sub> )	1263.5	0.71	-
Au@UiO-66(NH <sub>2</sub> ) <sup>c</sup>	1024.1	0.71	1.8 wt%
Au@UiO-66(NH <sub>2</sub> ) <sup>d</sup>	684.5	0.65	12.9 wt%

<sup>a</sup> All at nanoscale, <sup>b</sup> Modified literature procedure with 5.5 mmol Zn(NO<sub>3</sub>)<sub>2</sub>·4H<sub>2</sub>O, 2.0 mmol 2-aminoterephthalic acid and 50 mL DMF, <sup>c</sup> HAuCl<sub>4</sub> : MOF = 1:7.4, <sup>d</sup> HAuCl<sub>4</sub> : UiO-66(NH<sub>2</sub>) = 1:1

content in Au@UiO-66(NH<sub>2</sub>) was determined to be 1.6 wt% when 1:7.4 mole ratio of HAuCl<sub>4</sub> : UiO-66(NH<sub>2</sub>) was employed (Table 1). Nanoscale UiO-66(NH<sub>2</sub>) exhibited higher surface area during our investigation. The N<sub>2</sub> adsorption-desorption isotherms obtained at 77 K on the functionalized UiO-66(NH<sub>2</sub>) are type-I isotherms. UiO-66(NH<sub>2</sub>) and Au@UiO-66(NH<sub>2</sub>) possess similar patterns, which is indicated by similar surface areas and porosity (Fig. S7 and S8). The BET area only decreases from 1263.5 m<sup>2</sup>g<sup>-1</sup> to 1024.1 m<sup>2</sup>g<sup>-1</sup> after loading, while the gold content for Au@UiO-66(NH<sub>2</sub>) was determined to be 1.8 wt% (1:7.4 mole ratio of HAuCl<sub>4</sub> : UiO-66(NH<sub>2</sub>)). A catalyst with higher loading of gold content was achieved when the mole ratio of HAuCl<sub>4</sub> and UiO-66(NH<sub>2</sub>) was set to 1:1. Gold loading was measured to be 12.9 wt% according to ICP-AES (Table 1). The BET area further decreased to 684.5 m<sup>2</sup>g<sup>-1</sup> as the gold content was increased. This observation further confirms that the Au nanoparticles are mostly inside of the channel because of such a huge decrease in surface area. However, only 1.8 wt% gold catalyst was tested for its catalytic performance due to the cost of gold.

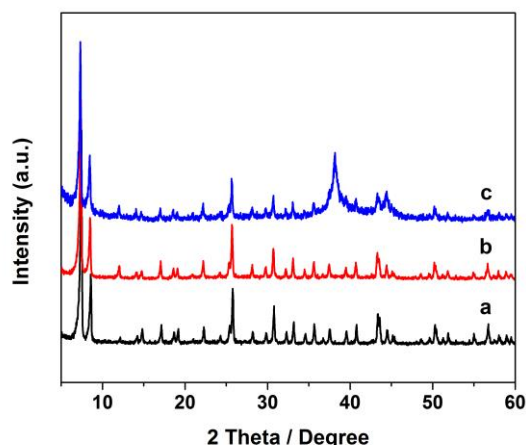


**Fig. 3** The powder XRD pattern of the UiO-66(NH<sub>2</sub>) (a) and 1.8 wt% and 12.9 wt% of Au@UiO-66(NH<sub>2</sub>) (b and c).

The powder XRD pattern of nanoscale UiO-66(NH<sub>2</sub>) is in agreement with previously reported UiO-66(NH<sub>2</sub>) materials in the literature (Fig. 3).<sup>40</sup> After the absorption of HAuCl<sub>4</sub> and NaBH<sub>4</sub> reduction, Au@UiO-66(NH<sub>2</sub>) showed no significant loss of crystallinity according to the powder XRD pattern, indicating that the framework of UiO-66(NH<sub>2</sub>) is mostly maintained. No diffractions were detected for gold nanocomposite, which indicate 1.8 wt% gold loading is too low for detection. At 12.9 wt% gold loading, a strong band at 38.2° is observed, which represents Bragg's reflections from (111) planes of Au. FTIR spectra indicate there is no component difference before and after gold loading, even when the gold loading went up to 12.9 wt% (Fig. S5). The UiO-66(NH<sub>2</sub>) and Au@UiO-66(NH<sub>2</sub>) MOFs were examined by thermal gravimetric analysis (TGA) to confirm the thermal and structural stability. The UiO-66(NH<sub>2</sub>) MOFs showed good thermal stability (Fig. S9). The gold deposited samples Au@UiO-66(NH<sub>2</sub>) show thermal stabilities comparable to that of UiO-66(NH<sub>2</sub>) with a decomposition temperature of approximately 400 °C in air (Fig. S10).

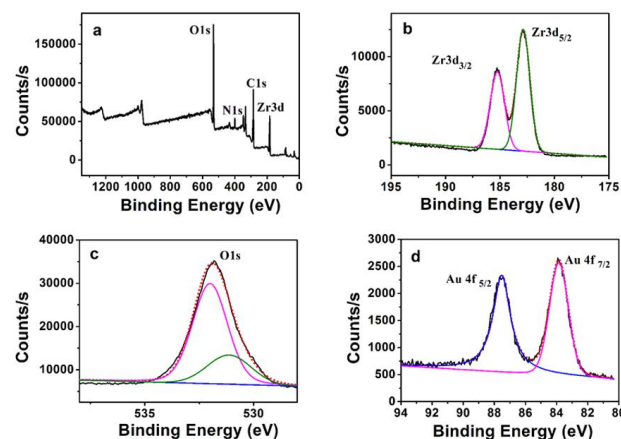


**Fig. 4** XPS patterns of 1.8 wt% Au@UiO-66(NH<sub>2</sub>) catalyst.

XPS measurements were carried out to analyze the surface chemical state of the as-synthesized 1.8 wt% Au@UiO-66(NH<sub>2</sub>). As presented in Fig. 4a, the XPS survey spectrum confirms the existence of Zr, Au, O, N and C in the sample. The signal strength of Au is low due to the relatively low loading of Au content in the MOF structure. The curves of Zr 3d region could be deconvoluted into two peaks for Zr 3d<sub>5/2</sub> and Zr 3d<sub>3/2</sub> located at around 182.9 eV and 185.2 eV, respectively. The deconvolution of the O 1s spectrum results in two peaks at 532.0 eV and 531.1 eV, which can be attributed to the carboxylate and other oxygen-containing species, respectively (Fig. 4). Furthermore, the oxidation state of the gold nanoparticles was confirmed. The Au 4f spectra shown in Fig. 4d fit the doublet of binding energy 87.5 eV and 83.8 eV attributed to Au 4f<sub>5/2</sub> and Au 4f<sub>7/2</sub> spin-orbit coupling of elemental gold (Au<sup>0</sup>), which indicates the formation of Au<sup>0</sup> nanoparticles through the reduction of AuCl<sub>4</sub><sup>-</sup> ions.

### 3.2. Aerobic Oxidations of Alcohols.

The selective oxidation of alcohols is one of the most important organic transformations in industry.<sup>41</sup> There are many oxidizing reagents for accomplishing such a transformation; however, a large percentage of these oxidants are highly toxic.<sup>42</sup> As the environmental concerns increase, more attention will be focused on the use of molecular oxygen as the oxidant.<sup>43</sup> Although aerobic oxidation of alcohols promoted by heterogeneous gold catalysts has been reported,<sup>44</sup> the application of supported gold nanoparticles in alcohol oxidation typically requires an aqueous alkaline reaction medium, such as excess NaOH or K<sub>2</sub>CO<sub>3</sub> solution. This caustic environment often results in undesired carboxylate products.<sup>45,46</sup> Our highly dispersed Au@UiO-66(NH<sub>2</sub>) catalyst offers great advantages in terms of high yield under base-free condition, as well as ease of catalyst synthesis, high catalytic efficiency and wide substrate tolerance.

The oxidations of alcohols were carried out under atmospheric O<sub>2</sub> pressure with the as-synthesized Au@UiO-66(NH<sub>2</sub>) catalysts. The aerobic oxidation of benzyl alcohol did not proceed in the absence of catalyst (Table 2, entry 1). 1.8 wt% Au@UiO-66(NH<sub>2</sub>) gave a low yield of the desired product due to slow conversion in acetonitrile at 80 °C (Table 2, entry 2). Significantly enhanced yields were observed using DMF as the solvent at a higher temperature, which is a common for aerobic alcohol oxidations (Table 2, entry 3).<sup>47</sup> UiO-66(NH<sub>2</sub>) support without nanomorphology control was tested. 1.8 wt% Au@bulk UiO-66(NH<sub>2</sub>) catalyst gave slightly lower yield in comparison to the nanoscaled heterogeneous catalysts (Table 2, entry 4). The better dispersion of the nanoscaled catalyst in solution was demonstrated in Fig. S3, which benefits liquid phase catalysis. These observations show the advantages of using nanoscaled MOF support in terms of catalytic performance. Higher gold catalyst loadings gave a comparable yield at much shorter reaction times (Table 2, entry 5). Overall, the use of 1.8 wt% Au@UiO-66(NH<sub>2</sub>) as the catalyst was found to be optimal due to the cost of gold. Unsupported gold nanoparticles, Au@TiO<sub>2</sub> and Au@PANI catalysts have been evaluated as controls in comparison of with the as-synthesized Au@UiO-66(NH<sub>2</sub>) catalyst. However, the unsupported gold catalyst did not function well in the absence of base under the optimized reaction conditions (Table 2, entry 6). The addition of Na<sub>2</sub>CO<sub>3</sub> boosted the yield to 15%, together with trace amount of ester by-product (Table 2, entry 7). Very low yield was obtained with Au@TiO<sub>2</sub> in the absence of Na<sub>2</sub>CO<sub>3</sub> base (Table 2, entry 8). Moderate yields were achieved when Na<sub>2</sub>CO<sub>3</sub> was utilized as the inorganic base (Table 2, entry 9). Furthermore, a slightly improved yield was observed with Au@PANI compared to Au@TiO<sub>2</sub>, which could be due to the basicity of PANI (Table 2, entry 10). The yield was further increased to 31% utilizing Na<sub>2</sub>CO<sub>3</sub> base (Table 2, entry 11). However, the catalytic efficiency is still significantly lower than the Au@UiO-66(NH<sub>2</sub>) system under base-free condition. The best results for aerobic oxidation of benzyl alcohol using our Au@UiO-66(NH<sub>2</sub>) catalyst were achieved in the absence of inorganic base (Table 2, entries 3). Our aerobic alcohol oxidation system is much more efficient than other literature reported gold heterogeneous systems,<sup>47,48</sup> which provides the desired aldehyde product in 38% yield using bulk gold catalyst and 9.2% yield using Au/MgO respectively. The reason for better catalytic performance is because of the highly dispersed gold nanoparticles in a large surface area

MOF support and the narrow distribution of gold nanoparticles without self-aggregation. The addition of a weak base, such as NaCO<sub>3</sub> and NaHCO<sub>3</sub> did not improve the conversion or yield (Table 2, entries 12 and 13).<sup>49</sup> It is also worth to mention that Au@UiO-66(NH<sub>2</sub>) catalyst tends to decompose slowly in the presence of weak inorganic base. The addition of strong base NaOH led to the decomposition of Au@UiO-66(NH<sub>2</sub>) catalyst, which formed a homogeneous solution at the end of the reaction and was the major reason for low conversion (Table 2, entry 14). We propose that the amino groups on the MOF act as a weakly basic promoter, which allows for the efficient aerobic oxidation catalyzed by Au@UiO-66(NH<sub>2</sub>) without the addition of a basic co-catalyst. Our base-free strategy extends the scope of available MOF supports since numerous MOFs are unstable toward inorganic bases.<sup>50</sup> The addition of radical initiators such as (2,2,6,6-tetramethyl-piperidin-1-yl)oxyl (TEMPO) or azobisisobutyronitrile (AIBN) did not affect the reaction rate, which suggests an anionic reaction pathway rather than the radical pathway (Table 2, entries 15 and 16).

**Table 2** Optimization of Aerobic Oxidation of Benzyl Alcohol<sup>a</sup>

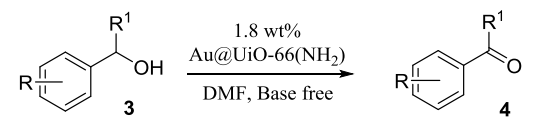
Entry	Catalyst	Solvent <sup>b</sup>	Additive	T [°C]	Yield <sup>b</sup>	Isolated Yield <sup>c</sup>
1 <sup>d</sup>	-	CH <sub>3</sub> CN	-	80	-	N.A.
2	Au@UiO-66(NH <sub>2</sub> )	CH <sub>3</sub> CN	-	80	17%	N.A.
<b>3</b>	<b>Au@UiO-66(NH<sub>2</sub>)</b>	<b>DMF</b>	-	<b>100</b>	<b>94%</b>	<b>91%</b>
4 <sup>e</sup>	Au@UiO-66(NH <sub>2</sub> )	DMF	-	100	78%	72%
5 <sup>f</sup>	Au@UiO-66(NH <sub>2</sub> )	DMF	-	100	93%	90%
6	unsupported Au	DMF	-	100	<5%	N.A.
7	unsupported Au	DMF	Na <sub>2</sub> CO <sub>3</sub>	100	15%	N.A.
8	Au@TiO <sub>2</sub>	DMF	-	100	8%	N.A.
9	Au@TiO <sub>2</sub>	DMF	Na <sub>2</sub> CO <sub>3</sub>	100	23%	14%
10	Au@PANI	DMF	-	100	23%	15%
11	Au@PANI	DMF	Na <sub>2</sub> CO <sub>3</sub>	100	31%	24%
12	Au@UiO-66(NH <sub>2</sub> )	DMF	Na <sub>2</sub> CO <sub>3</sub>	100	94%	N.A.
13	Au@UiO-66(NH <sub>2</sub> )	DMF	NaHCO <sub>3</sub>	100	94%	N.A.
14	Au@UiO-66(NH <sub>2</sub> )	DMF	NaOH	100	29%	N.A.
15	Au@UiO-66(NH <sub>2</sub> )	DMF	TEMPO	100	92%	N.A.
16	Au@UiO-66(NH <sub>2</sub> )	DMF	AIBN	100	92%	N.A.

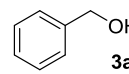
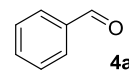
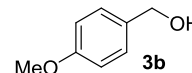
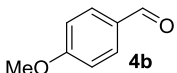
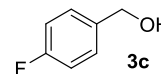
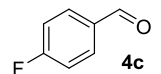
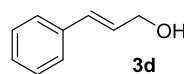
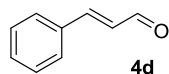
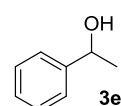
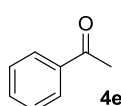
<sup>a</sup> Reaction conditions: benzyl alcohol (1.0 mmol), 1.0 mol% of 1.8 wt% Au@MOF catalyst, solvent (3.0 mL), 1 atm O<sub>2</sub> bubbling rate (20 mL/min) for 1 h, <sup>b</sup> Determined by GC-MS, <sup>c</sup> Isolated by column chromatograph, <sup>d</sup> Without catalyst, <sup>e</sup> 1.8 wt% Au@bulk UiO-66(NH<sub>2</sub>), <sup>f</sup> Using 12.9 wt% Au@UiO-66(NH<sub>2</sub>) for 10 min.

The catalytic performance of Au@UiO-66(NH<sub>2</sub>) was further evaluated in aerobic oxidations of various alcohols under the optimized reaction conditions. Benzyl alcohol **3a** was transformed to the desired benzaldehyde in 94% yield, which was confirmed through the isolated yield of 91% (Table 3, entry 1). This Au@UiO-66(NH<sub>2</sub>)-catalyzed aerobic oxidation approach was compatible with electron-rich aromatic alcohols, such as 4-methoxybenzyl alcohol **3b**.

The desired 4-methoxy benzaldehyde was isolated in 94% yield (Table 3, entry 2). For electron-deficient aromatic alcohol 4-fluorobenzyl alcohol **3c**, a slightly compromised yield was obtained under base-free conditions (Table 3, entry 3). Cinnamyl alcohol was evaluated as a vinylogous alcohol and great yield was achieved with the clean formation of cinnamaldehyde (Table 3, entry 4). Furthermore, 1-phenylethanol **3e** was tested as the model substrate for secondary alcohols, and a GC yield of 74% and isolated yield of 69% were obtained (Table 3, entry 5). It is worth mentioning that extended reaction times were not able to further increase the yield of acetophenone **4e**. The conversion of alcohol substrates over time was monitored by  $^1\text{H}$  NMR in DMF  $d_7$  solvent, which showed a clean formation of desired aldehyde products (see ESI).

**Table 3** Aerobic Oxidation Catalysis using Au@UiO-66(NH<sub>2</sub>)<sup>a</sup>



Entry	Substrate	Product	Yield <sup>c</sup>	Isolated Yield <sup>d</sup>
1			94%	91%
2			99%	94%
3 <sup>b</sup>			89%	86%
4			92%	90%
5			74%	69%

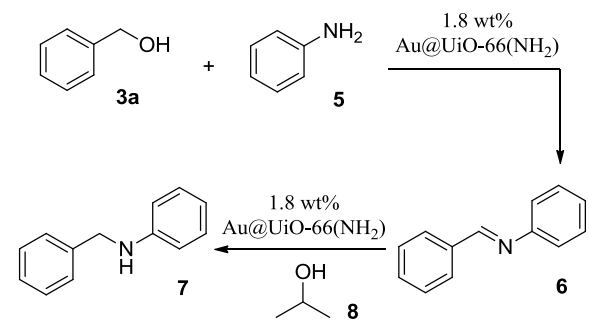
<sup>a</sup> Reaction conditions: alcohol (1.0 mmol), 1.0 mol% Au@UiO-66(NH<sub>2</sub>) catalyst, 3.0 mL DMF, 100 °C for 1 h, 1 atm O<sub>2</sub> bubbling rate (20 mL/min), <sup>b</sup> 6 h, <sup>c</sup> Determined by GC-MS, <sup>d</sup> Isolated by column chromatography.

### 3.3. N-alkylation of Primary Amines Reaction Sequences.

The reduction of 4-NP by NaBH<sub>4</sub> at room temperature was chosen as a test reaction to demonstrate the reduction activity of the Au@UiO-66(NH<sub>2</sub>) catalyst. The highly dispersed Au nanoparticles on UiO-66(NH<sub>2</sub>) showed excellent catalytic activity for the reduction of 4-nitrophenol using NaBH<sub>4</sub> as the reducing reagent. The reduction reaction did not proceed in the absence of catalyst or in the presence of only UiO-66(NH<sub>2</sub>) material.<sup>51</sup> A catalytic amount of 1.8 wt% Au@UiO-66(NH<sub>2</sub>) results in the full reduction of 4-nitrophenol to 4-aminophenol within 9 minutes (Fig. S18). As observed from the reaction solution, the bright yellow solution gradually became colorless. This observation demonstrated the high reactivity of

supported Au nanoparticles. Encouraged by the catalytic reduction and oxidation performance promoted by our 1.8 wt% Au@UiO-66(NH<sub>2</sub>), we hoped to further demonstrate the powerful reduction/oxidation activities of the gold heterogeneous catalyst. Therefore, we devised a reaction sequences involving an aerobic oxidation and a transfer hydrogenation reduction was designed. A amine *N*-alkylation reaction sequences employing benzyl alcohol **3a** and aniline **5** as the starting materials for generating secondary amines was studied.<sup>52,53</sup> This reaction reveals the ability of the Au@UiO-66(NH<sub>2</sub>) catalyst to promote both oxidations and reductions in the absence of O<sub>2</sub> and H<sub>2</sub>.<sup>54</sup>

**Table 4** Amine *N*-alkylation with alcohol via Oxidation/Imine Formation/Transfer Hydrogenation Reactions<sup>a</sup>



Entry	Conditions	Conv. of <b>3a</b>	Yield of <b>6</b>	Yield of <b>7</b>
1	No catalyst/DMF/100 °C	-	-	-
2	Au@UiO-66(NH <sub>2</sub> )/DMF/100 °C	18%	11%	5%
3	Au@UiO-66(NH <sub>2</sub> )/toluene/100 °C	39%	13%	21%
4 <sup>b</sup>	Au@UiO-66(NH <sub>2</sub> )/toluene/100 °C	99%	77%	14%
5	<b>Au@UiO-66(NH<sub>2</sub>)/xylenes/130 °C</b>	<b>76%</b>	<b>13%</b>	<b>53%</b>
6	Unsupported Au/xylenes/130 °C	14%	<5%	10%
7	Au@TiO <sub>2</sub> /xylenes/130 °C	23%	11%	10%
8	Au@PANI/xylenes/130 °C	38%	14%	19%

<sup>a</sup> Reaction conditions: aniline (1.0 mmol), benzyl alcohol (1.0 mmol), 2.0 mol% Au@UiO-66(NH<sub>2</sub>) (1.8 wt%) and solvent (2.0 mL) were stirred under N<sub>2</sub> atmosphere for 12 h, then 2-propanol (6.0 mmol) was added and the reaction was stirred for another 36 h, <sup>b</sup> Under O<sub>2</sub> atmosphere.

The *N*-alkylation of aniline **5** with benzyl alcohol **3a** over Au@UiO-66(NH<sub>2</sub>) catalyst was investigated in the presence of an excess amount of 2-propanol as a hydrogen donor and possibly a base (Table 4).<sup>54</sup> There was no imine or *N*-alkylation product in the absence of catalyst (Table 4, entry 1). 18% conversion of benzyl alcohol **3a** was achieved in the presence of Au@UiO-66(NH<sub>2</sub>) catalyst, however, only trace amount (5%) of *N*-benzylaniline **7** was produced with imine **6** as the major product (Table 4, entry 2). The formation of imine **6** excluded the possibility of direct *N*-alkylation from benzyl alcohol **3a** to *N*-benzylaniline **7**. A slightly higher conversion was achieved using toluene as the solvent under N<sub>2</sub> atmosphere (Table 4, entry 3). A full conversion of benzyl alcohol **3a** was observed under O<sub>2</sub> atmosphere. However, imine **6** was formed as the major product, together with only 14% of the desired

benzylaniline **7** (Table 4, entry 4). Lastly, xylenes was employed as the a higher boiling point solvent to boost the yield of the desired benzylaniline **7** to 53% (Table 4, entry 5). This is the one of few examples for the synthesis of *N*-benzylaniline **7** via a one-pot approach.<sup>55-57</sup> In contrast, unsupported gold nanoparticles, Au@TiO<sub>2</sub> and Au@PANI did not perform well under the optimal reaction condition (Table 4, entries 6-8). Au@PANI provided the highest conversion of the benzyl alcohol substrate **3a**, which leads to a 19% yield of the desired *N*-benzylaniline **7** product (Table 4, entry 8). Our system achieves much higher yield of *N*-benzylaniline **7** and employs no inorganic base. The yield of 53% is rather practical for the synthesis of *N*-benzylaniline, since a complicated organic transformation over three steps was carried out in a sequential reaction fashion.

### 3.4. Recycling of the Au@UiO-66(NH<sub>2</sub>) Catalyst.

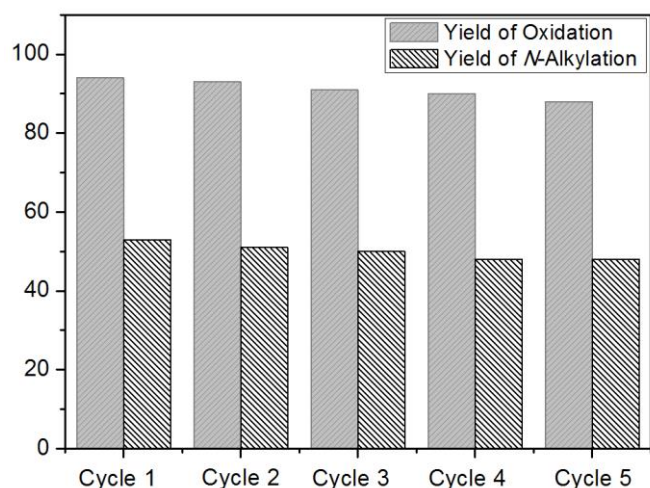


Fig. 5 Recycling of the Au@UiO-66(NH<sub>2</sub>) catalyst.

The recyclability of the Au@UiO-66(NH<sub>2</sub>) catalyst was evaluated employing the 1.8 wt% Au@UiO-66(NH<sub>2</sub>) catalyst for different organic transformations. For the aerobic oxidation of benzyl alcohol **3a**, only slightly lower yield were observed after over five runs (Fig. 5, Oxidation). The supernatant liquid of the DMF suspension showed no reactivity towards to the benzyl alcohol substrate, which indicates no leakage of the gold catalyst. This conclusion was further confirmed through ICP-AES analysis of the filtered supernatant liquid, which showed no gold content. The catalyst before and after catalysis was assessed by PXRD, FTIR and TEM to evaluate the structure integrity of the Au@UiO-66(NH<sub>2</sub>) catalyst. The PXRD and FTIR spectra of the Au@UiO-66(NH<sub>2</sub>) catalyst after used in five reactions times reuse were also indistinguishable from those of fresh catalyst (Fig. S5 and S13). Furthermore, SEM and TEM studies were carried out in order to show the stability of the catalyst morphology. There was no significant change in terms of nanomorphology of the as-synthesized catalyst after 5 cycles (Fig. S14). For the *N*-alkylation reaction sequences of aniline **5** with benzyl alcohol **3a** and, the

formation of desired secondary amine **7** showed almost no loss of reactivity after five runs (Fig. 5, *N*-alkylation).

## 4. Conclusions

In summary, highly dispersed Au nanoparticles deposited on amine-functionalized MOFs have been prepared through a facile solution-based synthetic approach. Nanomorphology was introduced to increase the dispersion of Au@UiO-66(NH<sub>2</sub>) catalyst in solvent, which resulted in high catalytic performance. The newly developed Au@UiO-66(NH<sub>2</sub>) catalyst served as an efficient nanocatalyst in the aerobic oxidation of alcohols and oxidation/imine formation/reduction reaction sequences. The Au@UiO-66(NH<sub>2</sub>) catalyst can be recycled five times without significant loss of activity in all catalytic reactions. Our rapid and facile synthetic approach opens up alternative routes for metal deposition on MOF catalysts under mild conditions, which can be utilized for a variety of catalytic organic transformations.

## Acknowledgements

We thank the National High Technology Research and Develop Program of China (863 program) (No. 2013AA031702) for financial support. Y. L. also thanks Beijing Natural Science Foundation (Grant No. 2144052) for financial support. We thank Dr. P. N. Moquist and Kathryn Summo (International Knowledge Editing) for helpful discussion and English editing.

## Notes and references

School of Materials Science and Engineering, University of Science and Technology Beijing, Beijing, 30 Xueyuan Road, 100083, P. R. China.  
E-mail: gewang@mater.ustb.edu.cn

† Electronic Supplementary Information (ESI) available: [EDX, FTIR spectrum, N<sub>2</sub> sorption/desorption isotherms, TGA, HRTEM]. See DOI: 10.1039/b000000x/

- 1 T. R. Cook, Y. R. Zheng and P. J. Stang, *Chem. Rev.*, 2013, **113**, 734.
- 2 H. Furukawa, K. E. Cordova, M. O'Keeffe and O. M. Yaghi, *Science*, 2013, **341**, 1230444.
- 3 A. Corma, H. García and F. X. Llabrés i Xamena, *Chem. Rev.*, 2010, **110**, 4606.
- 4 J. Y. Lee, O. K. Farha, J. Roberts, K. A. Scheidt, S. T. Nguyen and J. T. Hupp, *Chem. Soc. Rev.*, 2009, **38**, 1450.
- 5 D. Farrusseng, S. Aguado and C. Pinel, *Angew. Chem. Int. Ed.*, 2009, **48**, 7502.
- 6 P. Hervés, M. Pérez-Lorenzo, L. M. Liz-Marzán, J. Dzubiel, Y. Lu and M. Ballauff, *Chem. Soc. Rev.*, 2012, **41**, 5577.
- 7 J. Shan and H. Tenhu, *Chem. Commun.*, 2007, 4580.
- 8 M. K. Corbier, N. S. Cameron, M. Sutton, S. G. J. Mochrie, L. B. Lurio, A. Ruhm and R. B. Lennox, *J. Am. Chem. Soc.*, 2001, **123**, 10411.

## ARTICLE

- 9 P. Liu, Y. J. Guan, R. A. Santen, C. Li and E. J. M. Hensen, *Chem. Commun.*, 2011, **47**, 11540.
- 10 L. J. Shen, W. M. Wu, R. W. Liang, R. Lin and L. Wu, *Nanoscale*, 2013, **5**, 9374.
- 11 J. L. Long, H. L. Liu, S. J. Wu, S. J. Liao and Y. W. Li, *ACS Catal.*, 2013, **3**, 647.
- 12 H. L. Jiang, T. Akita, T. Ishida, M. Haruta and Q. Xu, *J. Am. Chem. Soc.*, 2011, **133**, 1304.
- 13 A. Dhakshinamoorthy and H. Garcia, *Chem. Soc. Rev.*, 2012, **41**, 5262.
- 14 H. L. Jiang, B. Liu, T. Akita, M. Haruta, H. Sakurai and Q. Xu, *J. Am. Chem. Soc.*, 2009, **131**, 11302.
- 15 H. L. Jiang, Q. P. Lin, T. Akita, B. Liu, H. Ohashi, H. Oji, T. Honma, T. Takei, M. Haruta and Q. Xu, *Chem. Eur. J.*, 2011, **17**, 78.
- 16 S. Hermes, M. K. Schröter, R. Schmid, L. Khodeir, M. Muhler, A. Tissler, R. W. Fischer and R. A. Fischer, *Angew. Chem. Int. Ed.*, 2005, **44**, 6237.
- 17 D. Esken, X. N. Zhang, O. I. Lebedev, F. Schröder and R. A. Fischer, *J. Mater. Chem.*, 2009, **19**, 1314.
- 18 H. R. Moon, D. W. Lim and M. P. Suh, *Chem. Soc. Rev.*, 2013, **42**, 1807.
- 19 M. Sabo, A. Henschel, H. Fröde, E. Klemm and S. Kaskel, *J. Mater. Chem.*, 2007, **17**, 3827.
- 20 Y. B. Huang, S. J. Liu, Z. J. Lin, W. J. Li, X. F. Li and R. Cao, *J. Catal.*, 2012, **292**, 111.
- 21 Y. K. Hwang, D. Y. Hong, J. S. Chang, S. H. Jung, Y. K. Seo, J. H. Kim, A. Vimont, M. Daturi, C. Serre and G. Férey, *Angew. Chem. Int. Ed.*, 2008, **47**, 4144.
- 22 Y. B. Huang, Z. L. Zheng, T. F. Liu, J. Lü, Z. J. Lin, H. F. Li and R. Cao, *Catal. Commun.*, 2011, **14**, 27.
- 23 Y. B. Huang, S. Y. Gao, T. F. Liu, J. Lü, X. Lin, H. F. Li and R. Cao, *ChemPlusChem*, 2012, **77**, 106.
- 24 M. Haruta, T. Kobayashi, H. Sano and N. Yamada, *Chem. Lett.*, 1987, **16**, 405.
- 25 M. Haruta, N. Yamada, T. Kobayashi and S. Lijima, *J. Catal.*, 1988, **115**, 301.
- 26 H. R. Moon, D. W. Lim and M. P. Suh, *Chem. Soc. Rev.*, 2013, **42**, 1807.
- 27 R. B. Wu, X. K. Qian, K. Zhou, H. Liu, B. Yadian, J. Wei, H. W. Zhu and Y. Z. Huang, *J. Mater. Chem. A*, 2013, **1**, 14294.
- 28 H. L. Liu, Y. L. Liu, Y. W. Li, Z. Y. Tang and H. F. Jiang, *J. Phys. Chem. C*, 2010, **114**, 13362.
- 29 L. H. Wee, M. R. Lohe, N. Janssens, S. Kaskel and J. A. Martens, *J. Mater. Chem.*, 2012, **22**, 13742.
- 30 E. A. Flügel, A. Ranft, F. Haase and B. V. Lotsch, *J. Mater. Chem.*, 2012, **22**, 10119.
- 31 M. Y. Masoomi and A. Morsali, *RSC Adv.*, 2013, **3**, 19191.
- 32 C. Carné, C. Carbonell, I. Imaz and D. Maspocho, *Chem. Soc. Rev.*, 2011, **40**, 291.
- 33 A. Carné-Sánchez, I. Imaz, M. Cano-Sarabia and D. Maspocho, *Nat. Chem.*, 2013, **5**, 203.
- 34 G. Lu, S. Z. Li, Z. Guo, O. K. Farha, B. G. Hauser, X. Y. Qi, Y. Wang, X. Wang, S. Y. Han, X. G. Liu, J. S. Duchene, H. Zhang, Q. C. Zhang, X. D. Chen, J. Ma, S. C. J. Loo, W. D. Wei, Y. H. Yang, J. T. Hupp and F. W. Huo, *Nat. Chem.*, 2012, **4**, 310.
- 35 M. Ma, D. Zacher, X. N. Zhang, R. A. Fischer and N. Metzler-Nolte, *Cryst. Growth Des.*, 2011, **11**, 185.
- 36 A. Schaate, P. Roy, A. Godt, J. Lippke, F. Waltz, M. Wiebcke and P. Behrens, *Chem. Eur. J.*, 2011, **17**, 6643.
- 37 M. Pintado-Sierra, A. M. Rasero-Almansa, A. Corma, M. Iglesias and F. Sánchez, *J. Catal.*, 2013, **299**, 137.
- 38 H. Wu, T. Yildirim and W. Zhou, *J. Phys. Chem. Lett.*, 2013, **4**, 925.
- 39 D. M. Jiang, A. D. Burrows and K. J. Edler, *CrystEngComm*, 2011, **13**, 6916.
- 40 M. Kandiah, S. Usseglio, S. Svelle, U. Olsbye, K. P. Lillerud and M. Tilset, *J. Mater. Chem.*, 2010, **20**, 9848.
- 41 A. Dhakshinamoorthy, M. Alvaro and H. Garcia, *Catal. Sci. Technol.*, 2011, **1**, 856.
- 42 R. A. Sheldon, I. W. C. E. Arends, G. T. Brink and A. Dijkstra, *Acc. Chem. Res.*, 2002, **35**, 774.
- 43 C. Parmeggiani and F. Cardona, *Green Chem.*, 2012, **14**, 547.
- 44 A. Corma and H. Garcia, *Chem. Soc. Rev.*, 2008, **37**, 2096.
- 45 L. Prati and F. Porta, *Appl. Catal. A: Gen.*, 2005, **291**, 199.
- 46 G. J. Hutchings, S. Carrettin, P. Landon, J. K. Edwards, D. Enache, D. W. Knight, Y. J. Xu and A. F. Carley, *Top. Catal.*, 2006, **38**, 223.
- 47 H. F. Guo, A. Al-Hunaiti, M. Kemell, S. Rautiainen, M. Leskela and T. Repo, *ChemCatChem*, 2011, **3**, 1872.
- 48 V. V. Costa, M. Estrada, Y. Demidova, I. Prosvirin, V. Kriventsov, R. F. Cotta, S. Fuentes, A. Simakov and E. V. Gusevskaya, *J. Catal.*, 2012, **292**, 148.
- 49 N. K. Chaki, H. Tsunoyama, Y. Negishi, H. Sakurai and T. Tsukuda, *J. Phys. Chem. C*, 2007, **111**, 4885.
- 50 N. F. Zheng and G. D. Stucky, *Chem. Commun.*, 2007, 3862.
- 51 W. C. Guo, Q. Wang, G. Wang, M. Yang, W. J. Dong and J. Yu, *Chem. Asian J.*, 2013, **8**, 1160.
- 52 J.-F. Soulé, H. Miyamura and S. Kobayashi, *Chem. Commun.*, 2013, **49**, 355.
- 53 Y. S. Lan, B. S. Liao, Y. H. Liu, S. M. Peng and S. T. Liu, *Eur. J. Org. Chem.*, 2013, 5160.
- 54 K. I. Shimizu, N. Imaiida, K. Kon, S. M. A. H. Siddiki and A. Satsuma, *ACS Catal.*, 2013, **3**, 998.
- 55 T. Ishida, N. Kawakita, T. Akita and M. Haruta, *Gold Bull.*, 2009, **42**, 267.
- 56 H. Liu, G. K. Chuah and S. Jaenicke, *J. Catal.*, 2012, **292**, 130.
- 57 S. Demir, F. Coşkun and İ. Özdemir, *J. Organomet. Chem.*, 2014, **755**, 134.